J Mater Sci (2011) 46:3753–3765
DOI 10.1007/s10853-011-5289-y

Longitudinal centrifugal casting of metal-matrix functionally graded composites: an assessment of modelling issues

A. Velhinho · L. A. Rocha

Received: 14 June 2010 / Accepted: 13 January 2011 / Published online: 29 January 2011

Abstract This study constitutes an effort to assess the relevant issues which should be addressed in order to adapt models currently available in the literature to predict final particle distribution resulting from radial centrifugal casting (CC) of particle-reinforced metal-matrix functionally graded composites (FGM) to the conditions prevailing in longitudinal CC. As such, a comprehensive review of a set of those models is performed, in order to ascertain the methodologies, the physical assumptions made, and the inherent limitations in applicability, so as to clearly identify the main deviations from the physical conditions prevailing during longitudinal CC. That review is then complemented by evidence of phenomena observed in longitudinally centrifuged FGM composites which are not in accordance with the physical assumptions admitted by the examined models, thus illustrating some of the issues which must be catered for in any successful effort to establish an adequate model for longitudinal CC.

Introduction

In many engineering applications, parts are subject to service conditions which vary considerably from point to point, demanding distinct types of performance from the constituent materials. However, it is well known that sharp variations in a material's composition or properties are liable to originate local stress concentrations, with negative consequences on the part's strength [1]. Such opposing circumstances have led to the definition and development of the functionally graded material (FGM) concept, a type of material exhibiting a continuous controlled variation of its composition and/or microstructure along at least one direction, in order to optimize its performance for a specific engineering application [2].

Although the FGM concept was only formally defined in Japan in the mid-1980's, as a result of the challenges placed by the airspace endeavour [1, 3], their practical use is, in some cases, rather ancient. Examples are the thermochemical treatment of steels in order to increase their superficial wear resistance through carburizing and nitriding, as well as the layer-by-layer assembly and heat-treatment of the traditional *katana* Japanese swords, all situations where the final part exhibits a gradual change in composition and microstructure [1].

Functionally graded materials can be seen as a different approach to the rationale used in the conceptualization of composite materials, which take advantage of the sometimes conflicting properties exhibited by different constituent materials in order to optimize the composite's overall properties. The main conceptual difference between composites and FGMs is that, while conventional composites are intrinsically heterogeneous, their macroscopic response can be regarded as homogeneous, even in those cases with a large degree of anisotropy. A FGM's heterogeneous nature, on the other hand, manifests itself at the macroscale, although in a gradual fashion, which sets these materials apart from a third category of non-homogeneous materials, which encompasses coatings, films and their abrupt junctions.

A. Velhinho (✉)
CENIMAT/I3N (Materials Research Centre/Institute for Nanostructures, Nanomodelling and Nanofabrication), Departamento de Ciência dos Materiais, Faculdade de Ciências e Tecnologia, FCT, Universidade Nova de Lisboa, 2829-516 Caparica, Portugal
e-mail: ajv@fct.unl.pt

L. A. Rocha
Centre for Mechanical and Materials Technologies (CT2M) and Department of Mechanical Engineering, University of Minho, Campus of Azurém, 4800-058 Guimarães, Portugal

Centrifugal casting as a method for FGM production

Centrifugal casting (CC) is a pressure solidification process where the metal is poured onto a rotating mould [4]. The prevailing metallostatic pressure thus results in better mould filling characteristics and reduced porosity content. Rohatgi et al. [5] mentioned examples of the application of CC to the processing of metal-matrix composites (MMC) occurring in the seventies; although pre-dating the definition of the FGM concept, some of those MMCs already distinguish themselves by the heterogeneous nature of the reinforcement distribution.

The production of functionally graded metal-matrix composites (FGMMC) through CC rests on the density difference between the composite constituents. The Stokes equation describes the velocity v_R imparted to an isolated spherical particle of diameter d_R and density ρ_R moving through a fluid of density ρ_L and intrinsic viscosity η when acted upon by an acceleration γ [1, 6–9]:

$$v_{\mathrm{R}} = \frac{d_{\mathrm{R}}^2(\rho_{\mathrm{R}} - \rho_{\mathrm{L}})\,\gamma}{18\,\eta_{\mathrm{L}}} \tag{1}$$

For the particular case of CC, the acceleration corresponds to $\gamma = \omega^2 r$ (ω being the angular velocity and r the distance between a given position and the rotation axis). By taking the gravitational acceleration g as reference [9]:

$$G = \frac{\gamma}{g} = \frac{\omega^2 r}{g} \tag{2}$$

As to the nature of γ, it should be noted that it is not necessarily centrifugal; in fact, it can just as easily correspond to the gravitational acceleration itself (G = 1), which leads to a treatment of gravity casting (GC)—in the course of which the settling (or floating) of the reinforcements is obtained—which parallels that of CC [7, 10]. In fact, those processes, i.e., CC and GC, are two of the most economically and technologically interesting methods available for FGMMC production [4, 8, 9, 11, 12]. Their implementation requires several steps [11]:

- the addition of the reinforcements to the molten metallic matrix, in order to obtain an homogeneous dispersion;
- the application of a centrifugal or gravitational field to the resulting slurry, in order to segregate the constituents and thus generate the intended gradient;
- the preservation of that distribution through the solidification of the slurry with a conveniently fast rate.

Regarding the technological options in CC, two kinds of equipment geometry have been described, with consequences on the orientation of the resulting gradients across the FGMMC part produced. The most frequent option corresponds to a radial geometry [4, 9, 11–16], where the mould's axis of symmetry coincides with the rotation axis. An alternative is the longitudinal geometry [8], corresponding to a configuration where the two axis are mutually perpendicular. In Fig. 1 schemes corresponding to those two alternatives are presented; the resulting orientation of the FGMMC gradients is also shown.

A key difference between the two CC configurations corresponds to the fact that, while the radial configuration allows the slurry to be poured onto an already rotating mould (whose velocity can, as a consequence, remain stable), the same situation is not possible with the longitudinal configuration: in this case, the centrifugal force must be applied simultaneously to the crucible as well as to the mould which, since they must remain fixed relative to each other, have to be kept stationary during melting; only after melting is completed can the rotation of the system be initiated, and as a consequence the applied centrifugal force varies with time during the operation, at least during a transient period.

Review of available spatial segregation models

Given the relevance of centrifugal casting for the production of FGMMCs, one may be surprised by the small number of models available in the literature to predict the reinforcement spatial segregation profiles resulting from the application of a centrifugal force to the melt. Some of the most representative of such models will now be briefly reviewed.

All the models studied for this study strive to equate two competing phenomena: ceramic particle travel throughout the metallic melt, which results from the differences of density between the composite constituents and from the acceleration imposed on the system, in accordance with the Stokes Eq. 1 prediction for each isolated (supposedly spherical) particle; and the progression of the matrix solidification front, which originates near the mould wall onto which the composite slurry is projected at the moment of pouring. It is from the balance established between these phenomena that the final particle distribution within the composite results.

Likewise, all the models assume a similar system configuration: they deal with radial geometries, and consider that the composite slurry is poured at temperature $T_P > T_{LIQ}$ onto a cylindrical mould with inner radius R_{i} and outer radius R_{e}, heated to a homogeneous temperature T_{M}, which rotates with a steady angular velocity ω around its cylindrical axis.

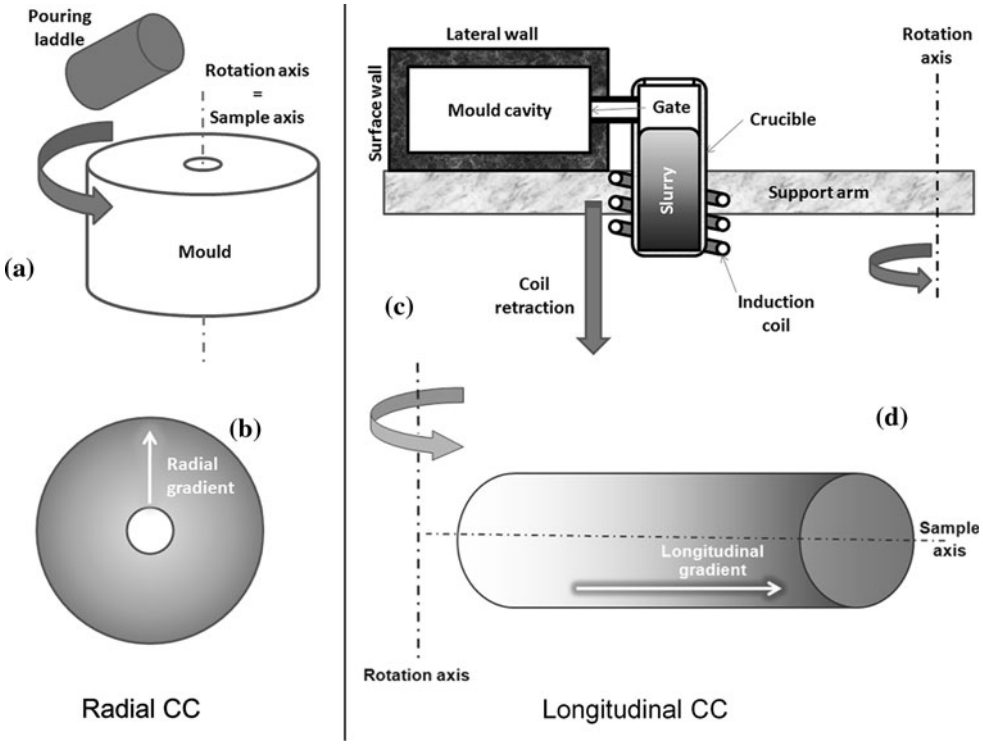

Fig. 1 **a** Radial CC furnace; **b** gradient orientation in a FGMMC processed by radial CC; **c** longitudinal CC furnace; **d** gradient orientation in a FGMMC processed by longitudinal CC

Lajoye and Suéry (LJ) model

The first model was proposed in 1988 by Lajoye and Suéry [6], and was based in a series of assumptions, which are presented in Table 1.

Based on those assumptions, the authors derive a set of equations describing the heat flow and the movement of each particle, which are then solved numerically in order to determine: (a) the variation in time of the temperature profile within the material and the mould; (b) the time-dependence of the solidification front velocity; (c) the resulting radial distribution profile of the reinforcement particles. However, this model has two shortcomings: the alloy latent heat of solidification is not accounted for in the heat flow calculation and the effect of the local variations in the melt temperature is not taken into account for the determination of the apparent viscosity η_{app} [17].

Kang and Rohatgi (KR) model

In order to address those shortcomings, Kang and Rohatgi have developed a different model [17]. For that purpose, these authors have considered a complex mould configuration, where an inner graphite mould of internal radius R_{ig} and external radius R_{eg} is enclosed by an outer steel casing of internal radius $R_{is} = R_{eg}$ and external radius R_{es}. Specific assumptions of this model are also presented in Table 1.

Two separate balances are established: a thermal balance, related to the progression of the solidification front, and a balance pertaining to the forces applied to each reinforcement particle, in order to establish its trajectory. The thermal balance is decomposed into a series of partial balances, each corresponding to a heat flow mechanism (conduction through the mould walls, the solidified part and the molten slurry; radiation through the inner cast ring wall). For that purpose, the thermo-physical properties (thermal conductivity, density and specific heat) of each region within the system are calculated through a rule of mixtures.

The numerical solutions for the set of balance equations are obtained by first establishing the individual position of each reinforcement particle, and then computing the thermal profile of the system for several instants. The resulting set of profiles is then used as a basis for determination of the solidification delay for every point in the cast part, as a function of the centrifugal acceleration, the mould initial temperature and the pouring temperature.

However, this model disregards the liquid displacement due to the particle motion, leading to a possible incongruence in the system mass balance. Also, the only means of coupling the particle motion and the progression of the solidification front is through the use in the thermal balance of the above mentioned rule of mixtures for the determination of the thermo-physical properties of the system constituents [11].

Table 1 A comparison of the assumptions made while deriving the models of Lajoye and Suéry (LS), Kang and Rohatgi (KR), Gao and Wang (GW) and Panda, Mazumdar and Mehrotra (PMM)

LS	KR	GW	PMM
The angular velocity is kept constant			
Heat flow occurs exclusively through the mould's circumferential outer wall; no losses occur through the top, bottom or inner walls.	Heat flow during solidification occurs through the graphite layer, into the steel casing, as well as through the inner wall of the cast ring, via a radiative process	Heat flow occurs exclusively through the mould's circumferential outer wall; no losses occur through the top, bottom or inner walls.	Heat flow during solidification occurs through the air gap into the graphite mould wall and then into a steel casing, as well as through the inner wall of the cast ring, via a radiative process
Heat flow is strictly unidirectional, perpendicular to the mould's outer wall			
Heat transfer to the mould is governed by a heat transfer coefficient h, which diminishes throughout the solidification process: $h = h_0 \left(\frac{h_f}{h_0}\right)^{\frac{e}{e_f}}$ (e thickness of the solidified layer; 0 initial state; f final state).	The heat transfer coefficient h is considered constant throughout the cooling process,		Due to the existence of an air gap between the mould wall and the cast part, heat transfer to the mould is governed by a heat transfer coefficient h, which diminishes throughout the solidification process: $h = h_0 \left(\frac{h_f}{h_0}\right)^{\frac{e}{e_f}}$ (e thickness of the solidified layer; 0 initial state; f final state).
Convection, buoyancy and gravity effects on the reinforcement particles are not considered.			Convection and buoyancy effects on the reinforcement particles are not considered.
The geometry of the solidification front can be locally considered as planar.			
The mould is instantaneously filled completely by the molten slurry with a homogeneous pouring temperature.			
–	There is no thermal resistance at the ceramic particle/melt interface.	Due to the metal's high thermal conductivity, thermal equilibrium is permanently maintained throughout the system.	There is no thermal resistance at the ceramic particle/melt interface.
Particle motion stops the instant it contacts the solidification front; particles do not move inside the mushy zone.			Particles do not move inside the mushy zone.
No particle-pushing by the solidification front.			Particle-pushing can occur
Due to the presence of a large number of particles, Stokes' equation can not be directly applied; for each particle, it needs to be corrected by locally computing the melt's apparent viscosity (η_{app}) as a function of the reinforcement particles volume fraction f_R.		A sedimentation rate for a multiparticle system is computed separately.	Similar to LS and KR.
A theoretical limit of 0.52 is adopted for f_R, due to particle packing considerations.	–	–	A theoretical limit of 0.52 is adopted for f_R, due to particle packing considerations.
Initially, the reinforcement particles are uniformly dispersed throughout the slurry.			
Similar to GW and PMM.	All the thermo-physical properties vary according to a rule of mixtures throughout the cooling process.	All the thermo-physical properties are considered constant throughout the cooling process, regardless of the temperature variation.	
Particle motion is slow.			
Particles are considered rigid spheres and are chemically inert towards the metal matrix.			
The system does not contain porosity.			

Gao and Wang (GW) model

In 2000, in an effort to improve the existing models, Gao and Wang [10, 11] developed an alternative model, whose assumptions can also be found in Table 1. Within the framework of the model, three different but coupled types of balances are established: mass balances, separately for the ceramic particles, the molten metal and the solidified matrix; momentum balances, separately for the reinforcement particles and the molten metal; and a common thermal balance, containing the heat contributions of every constituent phase within the system.

The combination of the different balance equations leads to solutions for the velocity of a reinforcement particle (v_R) and the velocity of the corresponding displaced liquid (v_L):

$$\begin{cases} |v_R| = \frac{(\rho_R - \rho_L)\, f_R\, \gamma\, d_R^2}{4\, \eta_L\, \beta^2\, (f_R + f_L)^2} \\ v_L = -\frac{f_R}{f_L}\, v_R \end{cases} \quad (3)$$

In Eq. (3), f_R and f_L stand, respectively, for the reinforcement particles and the molten metal volume fraction, β being given by Eq. (4):

$$\beta = \sqrt{\frac{9\,(1 - f_L)\, C}{2}} \quad (4)$$

with C corresponding to the sedimentation rate in the multiparticle system, a parameter related to the behaviour deviations of such a system (due to inter-particle collisions and to diverse particle morphologies and sizes) when compared to the ideal situation (single spherical particle) to which the Stokes Eq. (1) pertains [7, 10, 11]:

$$C = (1 - f_R)^{-4.65} \quad (5)$$

These parameters take into account the hindrance to particle motion caused by collisions while the rest of the reinforcement particles move through the melt (i.e., the effect of the particle population in the effective viscosity of the melt). As will be seen, this model needs several corrections in order to predict some experimental observations and to be able to cope with the special case of longitudinal centrifugal casting. However, it presents a comparative simplicity in terms of practical implementation, which makes it attractive as a stepping stone for more refined modelling.

Panda, Mazumdar and Mehrotra (PMM) model

More recently, a new alternative has been proposed by these authors [18] for the particular case of vertical axis radial centrifugal casting. Generally, the assumptions are comparable to those used for the preceding models, as can be see in Table 1, with small nuances such as, for instance, the allowance for gravitational effects, known to be present in the vertical configuration. More significantly, these authors include in the force balance a repulsive force term for the particles in the vicinity of the solidification front, thus allowing for the occurrence of particle-pushing effects, in line with common experimental observations for MMC casting techniques [19, 20].

In a similar fashion to the previously presented models, the particle segregation profile is derived through the combination of appropriate heat and force balances. However, from the implementation point of view, another significant distinction relative to the other models (which operate through finite-difference methods) is the fact that the authors have resorted to a finite-volume method.

Experimental

FGM fabrication

Precursor conventional MMCs, with a reinforcement volume fraction of 0.1, were rheocast from Al–10Si–2.2 Mg ingot material, which was reinforced by SiC particles. The chemical composition of the matrix alloy was controlled by optical emission spectroscopy, while a Coulter LS230 laser interpherometer was used to determine size distribution of the SiC particles added to the melt. Measured median particle sizes (D_V) of SiC reinforcements were 12.3, 37.4 and 118.8 μm, respectively. Details of the rheocasting apparatus and technique pertain to previous studies [21].

A high frequency induction centrifugal casting furnace (*Titancast 700* μP *Vac*, from Linn High Therm, Germany), equipped with a vacuum system, was then used for re-melting the precursor MMCs and casting the FGM samples. The furnace was instrumented in order to monitor and control the temperature of the melt, measure the rotational speed of the casting arm, and control the temperature of the mould. A schematic representation of the furnace layout is presented in Fig. 1c).

Unlike radial CC systems in which the liquid melt is poured into a rotating mould, in the equipment used in this study both the crucible and the mould are positioned in a centrifugal arm which rotates around a central axis. This system allows the production of cylindrical samples (40 mm diameter and 80 mm long), in which the gradient of particles is obtained at the surface of the cylinder, at the opposite side of the pouring hole. A charge of ca. 200 g of material was used in each experiment, which was always performed under vacuum ($p < 0.2$ Pa). After melting the material was poured into the mould as soon as the desired pouring temperature was achieved. The temperature of the melt was monitored and controlled by a chromel–alumel thermocouple (1.5 mm diameter) placed inside of an alumina tube. The thermocouple was connected to a *Shimaden FP21* controller. The material was poured into a graphite mould, which was placed inside a small furnace allowing the control of the temperature of the mould.

Figure 2a shows the evolution of the angular rotational velocity (ω) as a function of the position of the knob of the casting arm controller. Casting time was kept constant (90 s). As it can be seen, during casting the furnace allows a maximum angular rotational speed of 44 s^{-1}. The main difference between each position is related to the time taken by the motor to achieve the maximum speed, i.e., the

force associated to the torque (except for position 1 in which a maximum angular speed of 29 s^{-1} is achieved). The dependence of the acceleration with casting time is shown in Fig. 2b. As it can be seen, for position 1, acceleration varies continuously during casting, achieving a maximum of 11.5 g (112.6 m s^{-2}). A continuous evolution of the acceleration with casting time was observed for the other casting conditions, the difference being the achievement of a maximum acceleration of 24.5 g (240.4 m s^{-2}) some time after the rotation of the casting arm starts [8]. The time taken for the rotational arm to reach the maximum acceleration is called the delay time ($t_{\gamma MAX}$).

The processing conditions of the considered samples are presented in Table 2, where T_P is the pouring temperature and T_M is the mould temperature.

Table 2 Processing conditions of the FGMMCs considered for the present study

Condition	$t_{\gamma MAX}$ (s)	T_P (°C)	T_M (°C)	D_V (μm)	f_R	Matrix
A	5	850	25	12.3	0.1	Al–10Si–2 Mg
B	17					
I	5			37.4		
J	17					
K	5			118.8		
L	17					

Particle distribution profile determination

All samples were longitudinally cut in two halves, and polished for hardness measurements and metallographic examination. A good correlation has been found between the hardness of the material and the SiC particles area fraction determined by image analysis [8].

Quantitative analysis of the microstructure of the material was carried out in order to obtain information on particles area fraction and particle size distribution in depth. Image analysis was performed on grey scale digitized images (8 bit, 512 × 512 pixels), using an image analysis system developed at CEMUP (PAQI). Bright field images (×200) were first acquired by a TV camera attached to a *ZEISS Axioplan* reflection optical microscope. Images were captured at 2 mm intervals, both in the transverse and longitudinal directions of the samples. Image processing and segmentation prior to analysis involved a sequence of operations, repeated as a macro, including: delineation (for contrast and improved phase segmentation), thresholding (for particle segmentation into a binary image), morphological open-close filtering (for noise suppression), fill-holes filtering (for incomplete damaged carbide shape recovery) and finally particle de-agglomeration (for carbide particle separation, using a watershed based algorithm). In the final segmented (binary) image two main parameters were measured: particle surface fraction f_A—a stereological estimator of particle volume fraction f_R—and mean particle apparent diameter d_A—a stereological estimator of particle size d_R [8].

For each condition studied, average longitudinal profiles of f_A and d_A were obtained by taking into account the values measured in complete rows of micrographs corresponding to different samples—Fig. 3a). For the determination of transverse (radial) gradients, however, single samples were used, and on those samples narrow longitudinal strips of micrographs—A and B along the sample external regions, and C along the centre—were used to measure local f_A longitudinal profiles.

Results and discussion

Previous studies have shown that the influences of parameters such as the pouring and mould temperatures, the overall reinforcement particle volume fraction, the particle average size and the maximum acceleration during longitudinal CC are generally equivalent to what the available models would predict for similar variations in radial CC [8, 22–24].

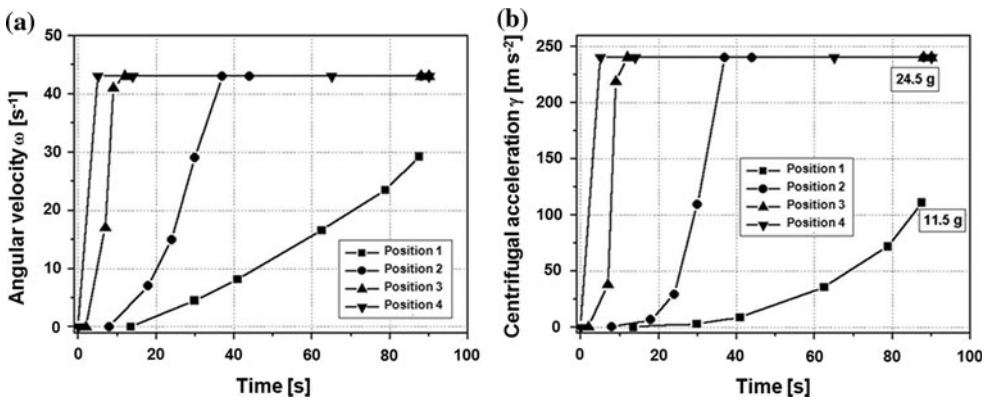

Fig. 2 [8] Casting conditions: **a** rotational angular velocity ω and **b** centrifugal acceleration γ as a function of casting time

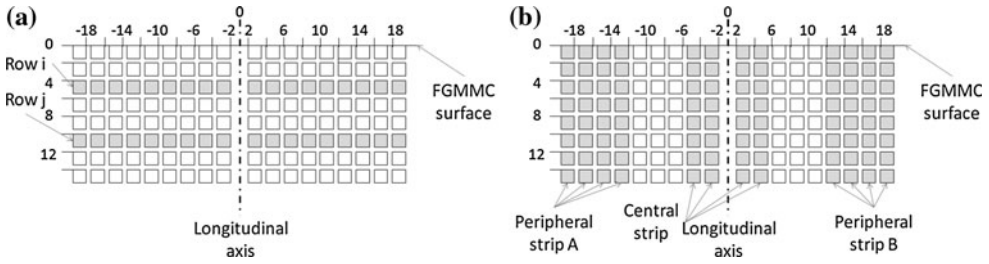

Fig. 3 Grid used for the QIA measurements. All values indicate positions in mm. **a** Rows of micrographs taken from several samples were combined and averaged to obtain overall longitudinal profiles of ceramic particle area fraction f_A and mean particle apparent diameter d_A along the FGMMCs. **b** Narrow longitudinal strips of micrographs taken from a single sample were used to obtain local longitudinal profiles of f_A, in order to study transverse segregation phenomena

Some observations, however, can only be explained beyond the scope of the existing modelling framework, as we shall now see.

Reverse segregation

Figure 4 shows the particle volume fraction and corresponding Vickers hardness profiles for the casting conditions mentioned in Table 2. It can be seen that in the cases of larger reinforcing particles or shorter delay times, a higher particle volume fraction is present near the FGM surface. In particular, for the combination resulting from the larger ($D_V = 118.0$ μm) particles and the severest casting conditions ($t_{\gamma MAX} = 5$ s), a particle-depleted zone is formed at just 12 mm below the FGM surface. Yet, for the mildest casting conditions ($t_{\gamma MAX} = 17$ s), a reverse gradient is noticeable near the FGM surface, with the maximum hardness value occurring at c. 10 mm below the surface.

A similar result had already been reported by Rocha et al. [8] for FGMMCs longitudinally cast from Duralcan precursors.

According to Stokes' Eq. 1, the primary factor governing the particle's segregation within the melt is the difference in densities ($\rho_{SiC} = 3.2$ g cm^{-3}; $\rho_{[Al]} = 2.3 \leftrightarrow 2.7$ g cm^{-3} [16, 19, 25]). That equation, however, also shows other influences, since larger particles will move with higher terminal velocities, as will particles subjected to higher centrifugal accelerations; conversely, the particle's motion will become slower if the melt viscosity increases. This means that, during the centrifugation cycle, each particle, if considered isolated, is under the action of two opposing forces: a centrifugal force, which impels it towards the surface of the FGM

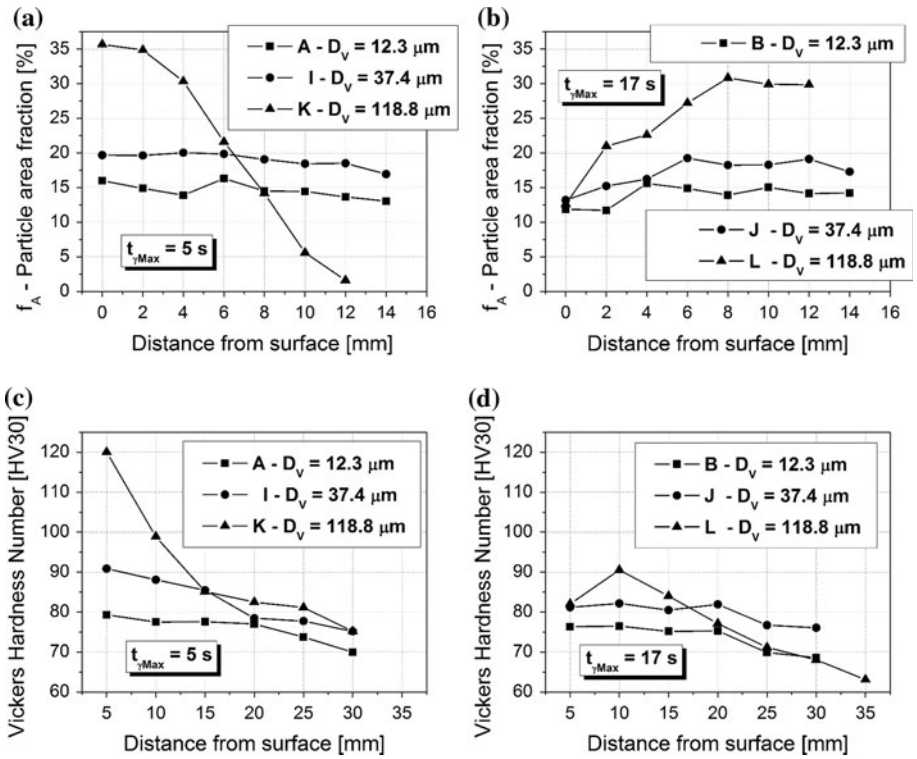

Fig. 4 [23] **a**, **b** Particle area fraction longitudinal profiles measured by quantitative image analysis of optical micrographs. **c**, **d** Vickers hardness longitudinal profiles. D_V represents the particles' median size

(considered as the region which solidifies in contact with mould wall opposite the gate), and a viscous drag force [6, 8, 14, 15, 22–24], which tends to oppose the particle's motion.

Gao et al. [10, 11] offer an expression for the viscous drag force by unit volume (M_R^D) acting upon a particle (f_L is the melt volume fraction and η_L is its intrinsic viscosity):

$$M_R^D = \frac{18\,(1 - f_L)\,\eta_L\,C}{d_R^2}\,f_L^2\,(v_L - v_R) \tag{6}$$

The parameter C is the sedimentation rate furnished by Eq. 5.

Concerning the viscous drag force, a different approach can be used for the melt viscosity. Apart from η_L being dependent on the alloy composition as well as its temperature, the melt's apparent viscosity (η_{app}) in the particle-containing slurry will be higher, precisely due to the presence of a given particle volume fraction (f_R).

Several approximations are proposed in the literature to express the dependence from f_R exhibited by η_{app}. According to Davis [26], if P_C represents a generic property of a composite (whose matrix is not necessarily in the solid state) containing a limited volume fraction f_R of reinforcement particles, the ration between P_C and the intrinsic value P_M of the property exhibited by the matrix will be given by the Einstein equation:

$$\frac{P_C}{P_M} = 1 + 2.5\,f_R \tag{7}$$

In the case of moderate inter-particle interactions, the series development of Eq. 7 leads to the introduction of a quadratic term, attributed by Davis [26] to such interactions:

$$\frac{P_C}{P_M} = 1 + \frac{5}{2}\,f_R + a_2\,f_R^2 \tag{8}$$

where a_2 is a function of the specific system and property under consideration.

However, the scope of this type of approach is necessarily limited, since as the value of f_R grows the contribution of the inter-particle interactions to the value of P_C is augmented in a non-linear fashion, requiring an increasing number of terms which may not be easy to determine [26].

Still, for the specific case of viscosity, several authors—among them Lajoye and Suéry for the development of their model—based on the approach embodied in Eq. 8, have proposed [1, 6]:

$$\eta_{app} = \eta_L\,\left(1 + 2.5\,f_R + 7.6\,f_R^2\right) \tag{9}$$

while others (including Kang and Rohatgi and Panda et al. in their models) prefer [17, 18, 27, 28]:

$$\eta_{app} = \eta_L\,\left(1 + 2.5\,f_R + 10.05\,f_R^2\right) \tag{10}$$

A different proposal can also be found [29] comprising an additional term (A and B are system-specific constants):

$$\eta_{app} = \eta_L\,\left(1 + 2.5\,f_R + 10.05\,f_R^2\right) + A\,\exp\,(B\,f_R) \tag{11}$$

A distinct approach is used by Brinkman [30], which introduces the concept of a theoretical maximum (f_{MAX}) for the particles volume fraction, based on the impossibility for non-parallelepiped particles to completely fill the available space. The proposed equation is:

$$\eta_{app} = \frac{\eta_L}{\left(1 - \frac{f_R}{f_{MAX}}\right)^{2.5}} \tag{12}$$

Equation 12 presents some similarities with an alternative proposal made by Davis [26], also for the generic property P_C, but in those situations where the intrinsic property value for the reinforcement particle (P_R) can be considered infinitely greater than P_M (a condition fulfilled by the viscosity when a molten metal contains a dispersion of ceramic solid particles):

$$\frac{P_C}{P_M} = \left(1 - \frac{f_R}{f_{MAX}}\right)^{-2.5\,f_{MAX}} \tag{13}$$

Incidentally, it should be noted that, while Lajoye and Suéry follow the Brinkman approach when considering a theoretical limit for f_R, those authors then revert to a simpler path, by using Eq. 8 in their calculations.

Eqs. 9–12 reveal the existence of a component of the viscous drag force which is generated by the particles themselves [8, 22, 24]—self-induced viscous drag.

However, there is another component of viscous drag. Indeed, while the ceramic particles travel along the mould, a continuous decrease in the melt temperature is occurring, eventually leading to the progression in the opposite direction of the solidification front. While theoretical models would in such situations predict the engulfment of the ceramic particles by the progressing solidification front, at least some experimental evidence pertaining to MMC casting indicates that particle-pushing is the more likely result when the two solid constituents meet each other [19, 20]. This effect of particle pushing constitutes a second contribution to the overall viscous drag [1, 6, 8, 14, 22, 24]—solidification viscous drag. This contribution provides the explanation for the occurrence of the reverse segregation, preventing further travel of the ceramic particles and leading to its accumulation some distance from the FGM surface. Yet, none of the models previously presented considers the possibility of particle-pushing.

Further consideration should be given to the influence on particle travel from particle effective size variations while travelling through the melt. In fact, while entering the solidification front neighbourhood, the ceramic particles are expected to act as heterogeneous nucleation sites for the matrix, with an increase in the effective size of the resulting cluster. If effective, this mechanism could compromise the applicability of the simple pushing versus engulfment theories. Not withstanding, when compared with the influence of solidification viscous drag on final particle distribution, as described before, such effect should probably be considered second-order. As such, it should not have to be dealt with until after coping with the main interaction between the ceramic particles and the advancing solidification front.

Another source of effective particle size variation would be the formation of a layer of reaction products if the composite constituents are not chemically inert (e.g., Al_4C_3 arising from the reaction between liquid Al and solid SiC). However, even in such a case, reaction kinetics might delay third-phase formation until the solidification process is effectively finished during the relatively brief CC cycle, which again should relegate such a consideration to a refinement stage in terms of model development.

Dimensional segregation

In Fig. 5 further measurements obtained through quantitative image analysis are presented, this time regarding the SiC particle size profiles within the FGM cast samples. Except for condition K ($D_V = 118.8$ μm; $t_{\gamma MAX} = 5$ s), when the largest particles are the ones that attain the surface, in all other cases there is peak in $d_R \equiv d_A$ occurring at some distance from the surface. Furthermore, increases in $t_{\gamma MAX}$ lead to decreased mean particle diameters at or near the surface. An exception exists regarding samples reinforced with $D_V = 12.3$ μm, in which an increase in mean particle diameter near the surface is obtained when less drastic casting conditions are used.

Similar evidence of dimensional segregation had already been presented by Rocha et al. [8] for longitudinally cast Al/SiC_p FGMMCs, as well as by Watanabe et al. [9, 12] for a model system made of a gypsum matrix containing corundum spheres and radially centrifuged.

The fact that dimensional dispersion is taking place is, before anything else, a clear indication of a measurable size distribution of the reinforcement particles. This aspect is never taken into account by the existing models, which assume that the entire particle population possesses a single diameter.

But the occurrence of dimensional segregation and its prevalence for the mildest casting conditions (longer $t_{\gamma MAX}$) is also a suggestion that the particle-pushing effect by the solidification front is more effective for the larger ceramic particles.

In fact, the solidification front can, as a first approximation, be thought of as originating at the mould wall

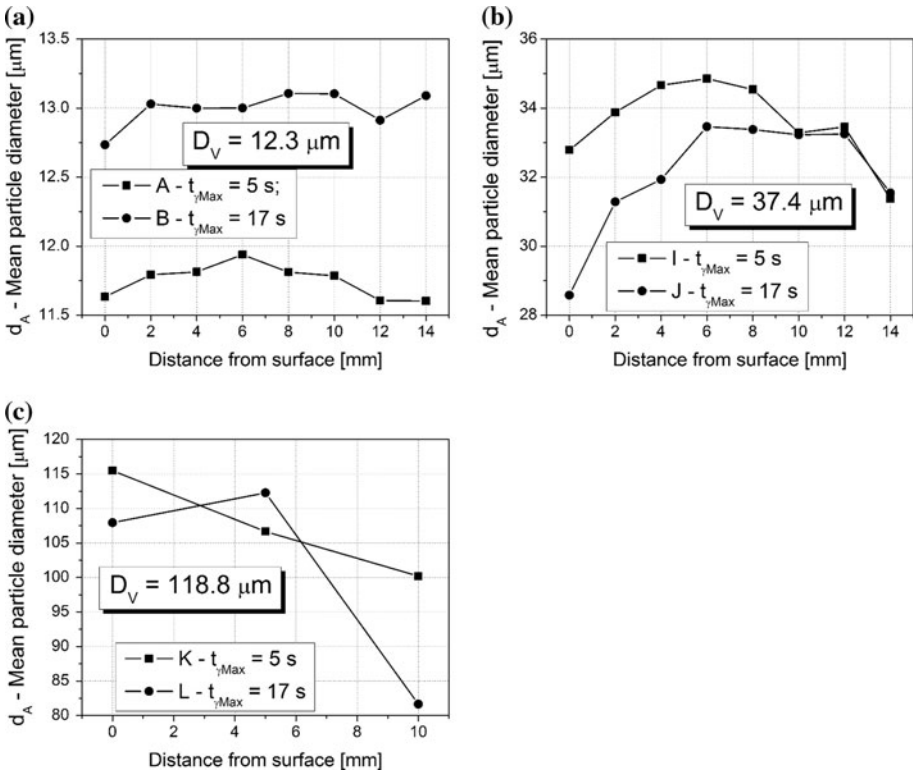

Fig. 5 [23] Mean particle diameter (d_A) longitudinal profiles, measured by quantitative image analysis of optical micrographs, for different particle median sizes (D_V): **a** $D_V = 12.3$ μm; **b** $D_V = 37.4$ μm; **c** $D_V = 118.8$ μm

opposite the gate by a nucleation mechanism, and progressing at the growth rate of the primary phase grains.

Until the eutectic temperature, liquid regions remain surrounding those grains. During the early stages of solidification, the solid volume fraction f_S will locally present very small values, with scarce solid–solid contact points, the solid being surrounded by a continuous liquid film. Under such circumstances, the solidification front will remain unconnected and behave as a non-newtonian fluid [26, 27].

However, as solidification proceeds, the value of f_S increases gradually, and the contacts between the primary phase grains become more common. Eventually a point of dendritic coherency is reached when the solid grains start forming a continuous skeleton, which nevertheless still possesses a network of inner channels filled with the remaining liquid [26, 28–30]; as a consequence, the solidification front will become more compact—but not planar, as all the available models have been considering—and will exhibit a selective permeability, determined by the relative abundance and cross-section of the interdendritic channels [31].

Dhale and Arnberg [32] suggest the Kozeny-Karman equation as a means to evaluate the permeability K of the solidification front:

$$K = \frac{(1-f_S)^3}{5\,(S_r f_S)^2} \qquad (14)$$

S_r being the specific surface area of the solid. The evolution of K with the increase of f_S is plotted in Fig. 6, for varying S_r values.

If the acceleration delay $t_{\gamma MAX}$ is brief, the reinforcement particles, particularly the largest ones, which acquire a greater velocity, are able to attain positions near the surface before the solidification front becomes too compact; thus, when the dendritic skeleton is finally formed, it does so around the particles already in place, effectively capturing them. For milder casting conditions, however, the advancement of the particles is opposed by a coherent solidification front, which pushes the larger particles towards the interior of the cast FGM, while momentarily still allowing the smaller particles to proceed their forward motion, eventually ending by being captured between the dendritic branches—Fig. 7. Thus, the velocity advantage conferred to the larger particles by their size only becomes effective if the casting conditions are sufficiently vigorous for them to reach near the FGM surface before a coherent solidification front has developed fully.

Transverse (radial) segregation

The primary intent when fabricating FGMMCs through the longitudinal CC process is to obtain a longitudinal gradient

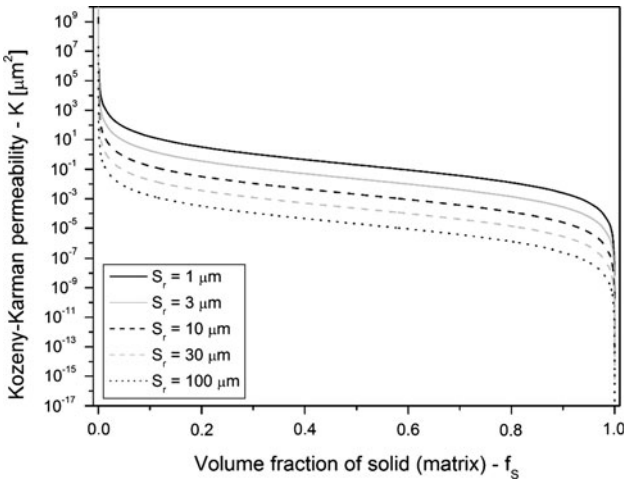

Fig. 6 Evolution of the Kozeny-Karman permeability (K) during solidification (f_S being the solid volume fraction in a two-phase system), considering different values for the solid-specific surface area S_r

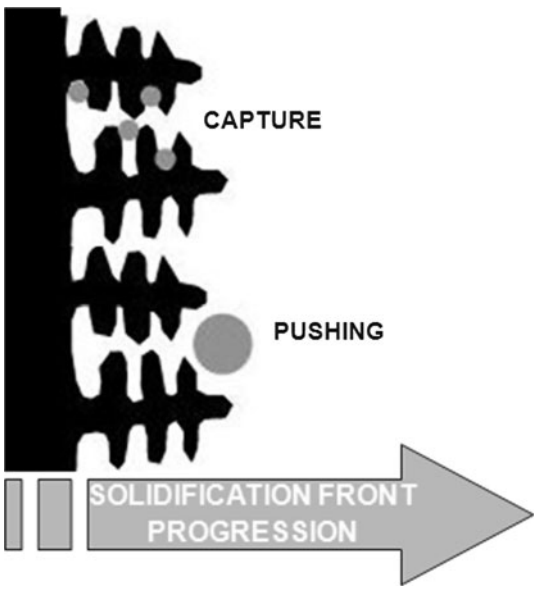

Fig. 7 Scheme illustrating the different possibilities for the interaction between a non-planar solidification front and the reinforcement particles, according to the particle size

of reinforcement particle distribution. However, as the graphs in Fig. 8, which compare overall f_R profiles with those measured along narrow longitudinal strips along the central axis and adjacent to the walls, clearly show, there seems to be a distinct transverse segregation of the particles, which are generally present in greater concentration in the central region. This transverse segregation is all the more noticeable when $t_{\gamma MAX}$ increases from 5 to 17 s, but does not seem to be much influenced by the average particle size.

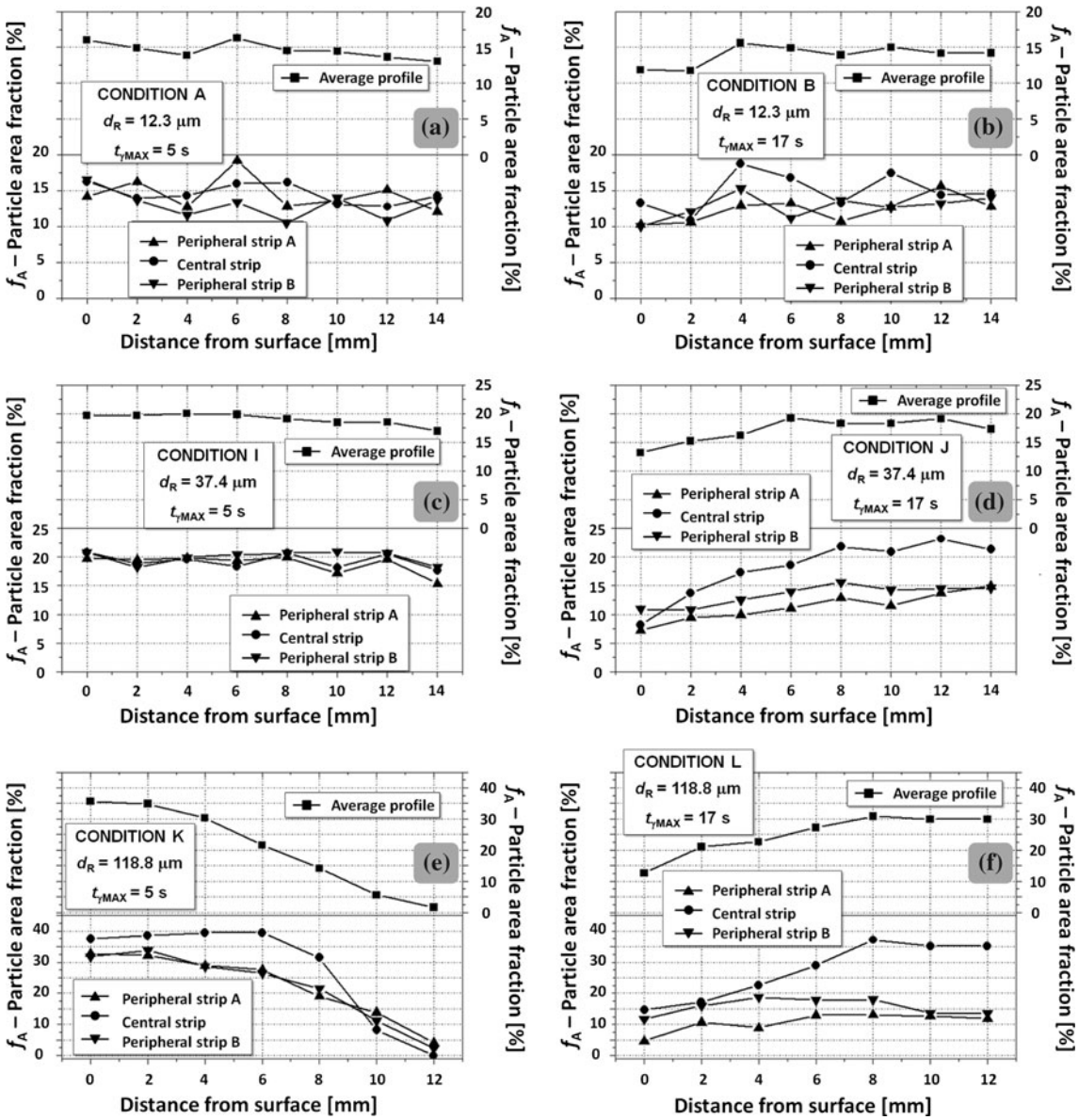

Fig. 8 Reinforcement particle area fraction (f_A) axial and peripheral longitudinal profiles, compared to the corresponding average profiles, for varying values of acceleration delay time ($t_{\gamma MAX}$) and average particle diameter d_R

Two distinct factors may contribute to the occurrence of radial segregation in longitudinally cast FGMMCs. A possible mechanism may be related to the complex shape of the solidification front within the longitudinal CC mould—Fig. 9a. Although the authors have previously only taken into account the mould wall opposite the gate as the site of solid nucleation, the reality is more complex, since immediately after pouring the slurry comes into contact with the lateral (cylindrical) mould wall. As a consequence, a secondary (radial) solidification front is formed, continuously disturbing the effect of the primary (longitudinal) solidification front by pushing the particles towards the central axis of the mould. This effect should be particularly marked, given the aspect ratio of the mould cavity used in this work's experiments (length = 80 mm; diameter = 40 m).

A second factor contributing to the radial segregation may simply be the transversal velocity profile of the slurry as it travels along the mould, as seen in Fig. 9b. The general theory of fluid flow inside a confined channel predicts a parabolic variation of the slurry velocity v with the distance to the mould wall, w, and the formation of a stagnant boundary layer near the lateral wall, which always presents a measurable roughness. As a result, the material progressing near the longitudinal axis of the mould is able to travel a longer path within each time increment, which

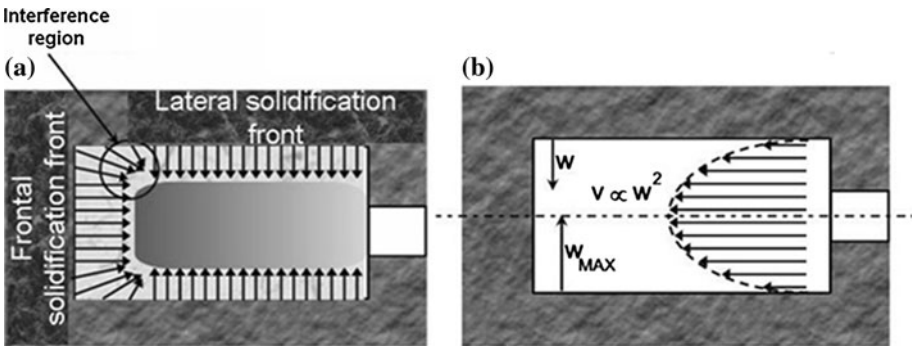

Fig. 9 Mechanisms of transverse segregation in longitudinal CC. **a** Apart from a primary (longitudinal) solidification front, a transverse centripetal solidification front progresses from the mould lateral wall. The resulting solidification viscous drag leads to an increased concentration of ceramic particles in the central region of the mould. **b** Transverse velocity profile of the slurry within the mould. The formation of a stagnant boundary layer near the mould lateral wall contributes to retard the material near that region, as compared to the material which travels along the central region, and thus further contributes to radial segregation

further contributes to the transverse segregation of the reinforcement particles. However, an exhaustive analysis of this effect is far from easy, since the continuous progression of the lateral solidification front effectively: (a) modifies the channel's diameter, dislocating the boundary layer and continuously modifying the velocity profile during the centrifugation cycle; (b) implies non-unidirectional heat and mass flows, thus dramatically altering the symmetry of the problem under consideration when trying to develop a predictive model for the process.

Conclusions

The task of developing a specific model for longitudinal centrifugal casting of particle-reinforced metal-matrix functionally graded composites must deal with the following issues, dictated by the observations above reported:

- first and foremost, the need to treat the centrifugal acceleration not as a constant, but as a variable governed by a time-law, as depicted indicated by the delay time $t_{\gamma MAX}$;
- the possibility of particle-pushing by the progressing solidification front, which is though to have implications in the observed reverse segregation and dimensional segregation effects;
- dimensional segregation also implies abandoning the single reinforcement particle diameter approach in favour of a finite particle size distribution;
- one further modification made necessary by the occurrence of dimensional segregation pertains to the selective permeability of the solidification front, whose morphology should be columnar/dendritic, instead of planar;
- a compound geometry for the solidification front, resulting from the coupling of a longitudinally progressing front generated at the mould wall opposite the gate and a radially progressing front generated at the lateral mould wall, becomes necessary if one is to predict effects like the observed transverse segregation; this modification transforms the problem's symmetry, since the heat and mass flows no longer can be considered unidirectional;
- the occurrence of a transverse velocity profile for the slurry as it feeds into the mould, which further contributes to the generation of transverse segregation gradients.

Acknowledgements Financial support by Fundação para a Ciência e Tecnologia (FCT—Portugal), under contract POCTI-CTM-56395-2004/PPCDT-CTM-56395-2004, is gratefully acknowledged.

References

1. Suresh S, Mortensen A (1998) Fundamentals of functionally graded materials - processing and thermomechanical behaviour of graded metals and metal-ceramic composites. The Institute of Materials, London
2. Gasik MM (2003) Mater Sci Forum 423–425:17
3. Uemura S (2003) Mater Sci Forum 423–425:1
4. Watanabe Y, Fukui Y (2000) Aluminum Trans 2:195
5. Rohatgi PK, Asthana R, Das S (1986) Int Mater Rev 31:115
6. Lajoye L, Suéry M (1988) In: Proceedings of international symposium on advances in cast reinforced metal composites. Chicago, USA, ASM International, p 15
7. Ourdjini A, Chew KC, Khoo BT (2001) J Mater Proc Technol 116:72
8. Rocha LA, Dias AE, Soares D, Sá CM, Ferro AC (2001) Ceramic Trans 114:467
9. Watanabe Y, Kawamoto A, Matsuda K (2002) Composites Sci Technol 62:881
10. Gao JW, Wang CY (2001) Trans of the ASME— J of Heat Trans 123:368
11. Gao JW, Wang CY (2000) Mater Sci Eng A A292:207
12. Watanabe Y, Fukui Y (2000) Recent Res Develop Metall Mater Sci 4:51
13. Watanabe Y, Eryu H, Matsuura K (2001) Acta Mater 49:775
14. Watanabe Y, Yamanaka N, Fukui Y (1998) Composites Part A 29A:595

15. Watanabe Y, Yamanaka N, Oya-Seimiya Y, Fukui Y (2001) Zeit fur Metallkunde 92:53
16. Rodríguez-Castro R, Wetherhold RC, Kelestemur MH (2002) Mater Sci Eng A A323:445
17. Kang CG, Rohatgi PK (1996) Metall Mater Trans B 27B:277
18. Panda E, Mazumdar D, Mehrotra SP (2005) Metall Mater Trans A 37A:1675
19. Clyne TW, Withers PJ (1995) An introduction to metal matrix composites. UK, Cambridge University, Cambridge
20. Kim JK, Rohatgi PK (2000) Metall Mater Trans A 31A p 1295
21. Velhinho A, Sequeira PD, Martins R, Vignoles G, Braz Fernandes FM, Botas JD, Rocha LA (2003) Nuclear Instr Method Phys B 200:295
22. Rocha LA, PD Sequeira, Velhinho A, Sá CM, (2001) In: Proceedings of XVI COBEM—Brazilian congress on mechanical engineering, Uberlândia, Brasil, p 381
23. Velhinho A, Sequeira PD, Fernandes FB, Botas JD, Rocha LA (2002) Mater Sci Forum 423–425:257
24. Velhinho A, Sequeira PD, Fernandes FB, Botas JD, Rocha LA, (2002) In: Proceedings of the XV CBECIMAT—Brazilian congress of Material science and Engineering, Natal, Brasil p 6
25. van Vugt L, Froyen L (2000) J Mater Proc Technol 104:133
26. Davis IL (1999) Curr Opin in Solid State Mater Sci 4:505
27. Lloyd DJ (1989) Composites Sci Technol 35:159
28. Lloyd DJ (1994) Int Mater Rev 39:1
29. Wang J, Guo Q, Nishio M, Ogawa H, Shu D, Li K, He S, Sun B (2003) J Mater Proc Technol 136:60
30. Brinkman HC (1952) J Chem Phys 20:571
31. Yang Y, Zhang Q, He Y, Hu Z (2001) Sci Technol Adv Mater 2:271
32. Dhale AK, Arnberg L (1996) J Mater 48:34